

Design of Nanovesicular Systems for Mangiferin Transdermal Delivery †

Maddalena Sguizzato ¹, Francesca Ferrara ², Paolo Mariani ³, Maria Grazia Ortore ³, Alessia Pepe ³, Rita Cortesi ¹, Mascia Benedusi ², Giuseppe Valacchi ^{2,4,5,*} and Elisabetta Esposito ^{1,*}

¹ Department of Chemical and Pharmaceutical Sciences, University of Ferrara, I-44121 Ferrara, Italy; sgzmdl@unife.it (M.S.); crt@unife.it (R.C.)

² Department of Neurosciences and Rehabilitation, University of Ferrara, Ferrara; I-44121 Ferrara, Italy; frrfnc3@unife.it (F.F.); bndmsc@unife.it (M.B.)

³ Department of Life and Environmental Sciences, Università Politecnica delle Marche, I-60131 Ancona, Italy; p.mariani@staff.univpm.it (P.M.); m.g.ortore@staff.univpm.it (M.G.O.); a.pepe@pm.univpm.it (A.P.)

⁴ Department of Animal Science, Plants for Human Health Institute, Animal Sciences Dept., NC Research Campus Kannapolis, NC State University, 28081, NC, USA

⁵ Department of Food and Nutrition, Kyung Hee University, Seoul 130-701, Korea

* Correspondence: vlcgpp@unife.it (G.V.); ese@unife.it (E.E.) Tel.: +39-0532-455230

† Presented at the 3rd International Online-Conference on Nanomaterials, 25 April–10 May 2022; Available online: <https://iocn2022.sciforum.net/>.

Abstract: Mangiferin is a natural antioxidant and anti-inflammatory agent suitable to treat skin diseases. To promote the transdermal administration of mangiferin, phospholipid based vesicular systems, ethosomes and transethosomes, were produced and characterized. The effect of polysorbate 80 and/or poloxamer 407 in transethosome composition was investigated on vesicles size distribution and morphology by photon correlation spectroscopy and transmission electron microscopy. Mangiferin encapsulation efficiency and in vitro diffusion parameters were evaluated by Franz cells. Mean diameter of vesicles was affected by phosphatidylcholine concentration and by the presence of polysorbate or poloxamer, ranging between 200 and 550 nm. A unilamellar supramolecular structure was detectable in the case of ethosome and polysorbate transethosome, while poloxamer led to multilamellar structures. The diffusion kinetic of mangiferin was faster in the case of transethosomes produced in the presence of poloxamer. Furthermore, 3D human skin models exposed to ozone demonstrated the antioxidant and anti-inflammatory effect of mangiferin containing transethosomes against pollutants, especially in the case of vesicles produced in the presence of poloxamer, suggesting their possible application to prevent and treat skin conditions associated to ox-inflammatory mechanisms.

Keywords: ethosomes; transethosomes; mangiferin; Franz cell; antioxidants

Citation: Sguizzato, M.; Ferrara, F.; Mariani, P.; Ortore, M.G.; Pepe, A.; Cortesi, R.; Benedusi, M.; Valacchi G.; Esposito, E. Design of Nanovesicular Systems for Mangiferin Transdermal Delivery. *Biol. Life Sci. Forum* **2022**, *2*, x. <https://doi.org/10.3390/xxxxx>

Publisher's Note: MDPI stays neutral with regard to jurisdictional claims in published maps and institutional affiliations.



Copyright: © 2022 by the authors. Submitted for possible open access publication under the terms and conditions of the Creative Commons Attribution (CC BY) license (<https://creativecommons.org/licenses/by/4.0/>).

1. Introduction

Air pollution is a main source of exogenous oxidative stress to which we are daily exposed, leading to a local or even systemic inflammatory status [1]. The chronic exposure to oxidants such as ozone can result in tissue damage including skin conditions [2]. To improve the natural immune defense, counteracting disorders induced by air pollution, natural antioxidants such as mangiferin (MG) can be employed. MG is a natural glucosyl xanthone possessing an antioxidant and anti-inflammatory activity, potentially suitable to prevent skin diseases exacerbation and/or development [3,4]. Since the peculiar morphology of the skin acts as a barrier to external insults, specialized delivery systems are required to promote transdermal drug passage through the skin, overcoming the stratum corneum and reaching the dermis. An innovative strategy for transdermal administration of drugs is typified by ethosomes (ETO). ETO are phosphatidylcholine

(PC) based nanovesicular systems that can be considered as a new generation of liposomes, possessing a similar composition, except for the presence of ethanol in relatively high concentration (30–45%). The rationale of using ethanol is related both to technological as well as to biological advantages. Indeed, the presence of ethanol contributes to improve the solubility of lipophilic molecule and to stabilize the dispersion, avoiding the use of preservative agents. In addition, ethanol makes the vesicle malleable improving their capability to pass through the physiologic membranes, while promoting the vesicle transdermal passage thanks to its penetration enhancing property [5]. The ETO vesicles are constituted of PC organized in double layers embedding ethanol and the solubilized lipophilic drugs. To further modify the vesicle structure, possibly improving their transdermal efficacy, ETO can be enriched with surfactants, resulting in the so-called transtethosomes (TETO) [6]. In the present study ETO and TETO were investigated as transdermal delivery systems for MG. Particularly, ETO and TETO were characterized for their morphology, size distribution and capability to entrap MG. The MG diffusion profile was investigated *in vitro* by Franz cells, while 3D human skin models exposed to ozone were employed to evaluate the antioxidant and anti-inflammatory effect of MG containing ETO and TETO against pollutants.

2. Materials and Methods

Mangiferin (MG), the copolymer poly(ethylene glycol)-block-poly(propylene glycol)-block-poly(ethylene glycol) poloxamer 407 (P407) (PEO98-POP67-PEO98), and polysorbate 80 (TW₈₀) were purchased from Sigma-Aldrich (St Louis, MO, USA). The soybean lecithin (PC) (90% phosphatidylcholine) was Epikuron 200 from Lucas Meyer (Hamburg, Germany). Nylon membranes were purchased from Merck (Milan, Italy). Solvents were of HPLC grade, and all other chemicals were of analytical grade.

Vesicular nanosystems were prepared by the addition of bidistilled water into an ethanolic solution of PC (90% w/v) [7]. Namely, to prepare ETO, water was slowly added to the ethanol phase up to a final water/ethanol ratio of 20:80 or 70:30 (v/v), under magnetic stirring at 750 rpm (IKA RCT basic, IKA®-Werke GmbH & Co. KG, Staufen, Germany) for 30 min at room temperature. In the case of TETO preparation, TW₈₀ or P407 were respectively solubilized in the PC ethanol solution before water addition. MG containing nanosystems were prepared, solubilizing the drug (1 mg/mL) alternatively in the PC, PC/TW₈₀, or PC/ P407 ethanol solution, before adding water.

Size analysis of vesicular nanosystems was performed by Photon Correlation Spectroscopy (PCS) using a Zetasizer Nano-S90 (Malvern Instr., Malvern, UK) equipped with a 5 mW helium neon laser and a wavelength output of 633 nm. Measurements were performed at 25 °C, 90° angle, and a run time of at least 180 s. After sample dilution with bidistilled water (1:20 v/v ratio), the experimental intensity autocorrelation functions were measured and analyzed using the “CONTIN” method that enabled to calculate the mean hydrodynamic diameter for each population [8]. Measurements were repeated thrice on different samples.

For morphological analyses, Transmission Electron Microscopy (TEM) was employed. Samples were negatively stained, depositing a sample drop on a TEM screen covered with a Formvar film (Media System Lab S.r.l., Macherio, MB, Italy). The excess drop was removed after 1 min from the screen with filter paper to keep a light veil of sample on the supporting substrate. A drop of 2% phosphotungstic acid was placed on the screen for 1 min and then removed with filter paper to surround the nanosystems deposited on the screen and adhere to their surface. The screen was then observed with a ZEISS EM 910 transmission electron microscope (Carl Zeiss Microscopy, GmbH, Munich, Germany).

Small and Wide-Angle X-ray scattering (SAXS and WAXS) experiments were conducted at the I22 beamline of Diamond Light Source (Harwell, UK). The experiment exploited the mail-in service. The 3m camera anisotropic SAXS/WAXS I22 setup and a Pilatus P3-2M (Silicon hybrid pixel detector, DECTRIS) detector with a pixel size of 172

μm^2 were used. The final investigated Q-range was 0.4–3.0 nm^{-1} for SAXS and 3.0–50 nm^{-1} for WAXS. Samples were prepared in a capillary rack, each capillary having a diameter of 1 mm. Two-dimensional (2D) data were corrected for background, detector efficiency, and sample transmission, and then radially averaged to derive $I(Q)$ vs. Q curves [9].

To evaluate MG entrapment capacity (EC), 500 μl of each sample were loaded in a centrifugal filter (Microcon centrifugal filter unit YM-10 membrane, NMWCO 10 kDa, Sigma-Aldrich, St. Louis, MO, USA) and ultra-centrifuged (Spectrafuge™ 24D Digital Microcentrifuge, Woodbridge, NJ, USA) at 4,000 rpm for 15 min. Afterwards, a 100 μl aliquot of supernatant (in the upper section of the filter unit) was diluted with ethanol (1:10, v/v) and maintained under magnetic stirring for 30 min [7]. After filtration of the solution by nylon syringe filters (0.22 μm pores), MG amount was analyzed by HPLC as below reported. The EC was determined as follows:

$$\text{EC} = \text{MG} / \text{T}_{\text{MG}} \times 100, \quad (1)$$

where MG is the amount of drug measured by HPLC and T_{MG} is the total amount of MG employed for nanosystem production.

In vitro MG diffusion from ETO-MG and TETO-MG was investigated by Franz cells assembled with nylon membranes (2 cm diameter, pore size 0.2 μm) (Vetrotecnica, Padova, Italy) [10]. Franz cells were set up of a lower receptor and an upper donor compartment separated by a membrane, whose exposed surface area was 0.78 cm^2 (1 cm diameter orifice). Before starting the experiment, the membranes were hydrated with the receiving phase for 1 h. Five milliliters of ethanol/water (50:50, v/v) were poured in the lower section, stirred at 500 rpm by a magnetic bar and thermostated at $32 \pm 1^\circ\text{C}$ during all the experiments [11]. Approximately 1 g of MG containing forms was placed in the donor compartment sealed to avoid evaporation. At predetermined time intervals (0.5–6 h), 200 μl of receiving phase were withdrawn, replaced with an equal volume, and analyzed for MG content by HPLC. The MG concentrations were determined six times in independent experiments and the mean values \pm standard deviations were calculated. The accumulation curves were obtained plotting mean values as a function of time. The fluxes were extrapolated from the linear portion of the curves, considering the slopes of the regression line (angular coefficient). At last, the diffusion coefficients were calculated according to Equation (2).

$$D = F / [\text{MG}], \quad (2)$$

where D is the diffusion coefficient, F is the flux and [MG] is the MG concentration in the analyzed form, expressed in mg/ml.

HPLC analyses were performed by a two-plungers alternative pump (Agilent Technologies 1200 series, Santa Clara, CA, USA), an UV-detector operating at 254 nm, and a 7125 Rheodyne injection valve with a 50 μL loop. A stainless-steel C-18 reverse-phase column (15 \times 0.46 cm) packed with 5 μm particles (Platinum C18, Apex Scientific, Alltech, Nicholasville, KY, USA) was eluted by a mobile phase containing methanol/water 60:40 v/v, pH 4.0 at a flow rate of 1 mL/min.

For biological studies, EpiDerm (EPI-200) skin model samples were obtained from MatTek corporation (Ashland, MA, USA) and transferred into 6-wells plates prefilled with 1 ml of MatTek assay medium upon arrival, following the Manufacture's protocol [12]. After 24 h of recovery in incubator (5% CO_2 , 37 $^\circ\text{C}$), 1 ml of fresh new medium was added to each well to topically pretreat the tissues with 35 μL of vesicular nanosystems for 24 h. Afterwards vesicular nanosystems were placed in a plexiglass box connected to an ozone (O_3) generator equipped with a detector able to monitor the O_3 concentration and exposed to 0.4 ppm of O_3 for 4 h, as previously described [12]. Inserts and media were collected directly after exposure (0 h) or 24 h post-exposure. Untreated tissues exposed to O_3 at the same conditions were used as reference, while untreated tissues exposed to filtered air were used as control (CTRL).

Sections of EpiDerm skin model were previously fixed in formalin, then embedded in paraffin (formalin-fixed paraffin-embedded, FFPE) and finally subjected to immunofluorescence staining for 4-hydroxy-nonenal (4HNE). Briefly, 4 μm sections were deparaffinized, rehydrated, and incubated in a 10 mM citrate buffer pH 6 (AP-9003-500, Thermo Fisher Scientific, Waltham, MA, USA) at 90 °C for 10 min in a 500-watt microwave for the antigen retrieval step. After cooling for 30 min at RT, sections were firstly washed twice in phosphate buffer saline (PBS), then blocked for 45 min in PBS containing 2% bovine serum albumin (Biorad, Hercules, CA, USA) and further incubated overnight at 4 °C with 4-HNE antibody diluted 1:400 in PBS, BSA 0.2% (AB46545, Abcam, Burlington, MA, USA). Tissue sections were then washed 3 times in PBS before incubation with secondary antibody Goat Anti-rabbit IgG H&L (Alexa Fluor® 488; A-11008, ThermoFisher scientific, Cambridge, UK) (1:1000 in PBS, BSA 0.2%) for 1h at 25 °C. After washing in PBS, nuclei were stained with a diamidino-2-phenylindole dye DAPI (Tocris Biosciences, Bristol, UK) 300 mM solution for 5 min, then washed again in PBS. Coverslips were subsequently mounted onto glass slides using the Permafluor aqueous mounting medium (ThermoScientific™, Minneapolis, MN, USA) and consequently imaged via fluorescence on a Nikon Microphot FXA microscope (Nikon Instruments, Amsterdam, Netherlands) equipped at 40x magnifications. Fluorescence staining intensity was quantified using Imagej software [13]. After collecting the tissues media at the two different time-points upon O₃ exposure (0 and 24 h), IL-1 β levels were measured by using the Human IL-1 beta/IL-1F2 DuoSet ELISA kit (R&D System cat DY201, Minneapolis, MN, USA), according to the manufacturer's protocol. IL-1 β levels were adjusted for media (pg/mL) and expressed as arbitrary units (AU %). Gen5 software (BioTek, USA) was used for the detection [12].

3. Results

3.1. Ethosome and Transethosome Preparation

With the aim to design topical formulations suitable for MG solubilization and delivery through the skin, biocompatible vesicular nanosystems containing high amounts of ethanol, were prepared [7]. Particularly, the nanosystem composition was mainly based on PC (0.9 or 1.8%) and ethanol 30%, resulting in the production of ETO, while the enrichment of ETO composition with TW₈₀ (0.2 or 0.3%) or P407 (1.2%) led to TETO (Table 1). The vesicular dispersions appear homogeneous and milky, translucent in the case of TW₈₀ presence. The loading of MG did not affect the macroscopic aspect of ETO and TETO.

Table 1. Composition of ethosomes and transethosomes.

Formulation	PC ¹ % w/w	Ethanol % w/w	TW ₈₀ ² % w/w	P407 ³ % w/w	MG ⁴ % w/w	Water % w/w
ETO	0.9	29.1	-	-	-	70.0
ETO-MG	0.9	29.1	-	-	0.1	69.9
TETO 1	0.9	28.8	0.3	-	-	69.9
TETO 1-MG	0.89	28.8	0.3	-	0.1	69.9
TETO 2	1.8	17	-	1.2	-	80.0
TETO 2-MG	1.8	16.9	-	1.2	0.1	80.0
TETO 3	1.8	18	0.2	-	-	80.0
TETO 3-MG	1.8	17.9	0.2	-	0.1	80.0

¹ phosphatidyl choline; ² polysorbate 80; ³ poloxamer 407; ⁴ mangiferin.

3.2. Ethosome and Transethosome Characterization

In order to study the influence of the composition on ETO and TETO physico-chemical aspect, size distribution and morphology of vesicular nanosystems were evaluated. Particularly the size distribution, studied by PCS revealed that Z-Average mean diameters were comprised between 170 and 340 nm, as a function of composition (Table 2). The

smallest Z-Average mean diameter was found in the case of vesicles produced in the presence of low amounts of PC and TW_{80} (TETO 1), while the largest one was obtained by the use of a higher amount of PC and lower amount of TW_{80} (TETO-3). The presence of P407 resulted in vesicles whose mean diameter was almost 50 nm larger with respect to ETO (TETO-2). The addition of MG in ETO and TETO led to a slight reduction of mean diameters. In all cases dispersity indexes were below 0.2, reflecting a narrow size distribution, characterized by almost one vesicle population, as indicated by the typical intensity distribution values.

Table 2. Size distribution parameters of ethosomes and transethosomes, as determined by PCS.

Formulation	Z-Average (nm) \pm s.d. (nm)	Typical Intensity distribution		Dispersity index \pm s.d. (nm)
		nm	Area %	
ETO	206.3 \pm 33	261 (5065)*	99.5 (0.5)*	0.14 \pm 0.04
ETO-MG	189.8 \pm 13	178.8 (5049)*	99.6 (0.4)*	0.13 \pm 0.02
TETO-1	186.2 \pm 20	187.0	100	0.13 \pm 0.05
TETO-1-MG	169.3 \pm 1	168.7	100	0.13 \pm 0.02
TETO-2	253.3 \pm 25	255.3	100	0.18 \pm 0.04
TETO-2-MG	243.7 \pm 22	245.2	100	0.17 \pm 0.03
TETO-3	338.5 \pm 30	336 (1080)*	99.5 (0.5)*	0.18 \pm 0.05
TETO-3-MG	332.5 \pm 25	320 (2040)*	99.4 (0.6)*	0.20 \pm 0.05

* Secondary peak.

The morphology of vesicular nanosystems, evaluated by TEM, showed roundish vesicles, whose mean diameters reflected Z-Average values measured by PCS. Figure 1 reports representative images of TETO produced in the presence of MG. Particularly in the case of TETO-2 (Figure 1a) multilayered strata can be observed at the vesicle interface.

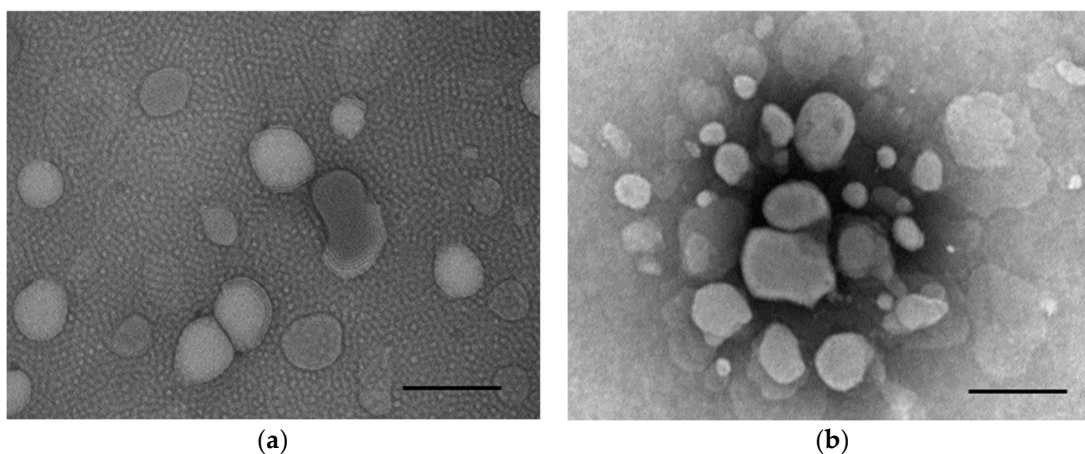


Figure 1. Transmission electron microscopy images (TEM) of TETO-2-MG (a) and TETO-3-MG (b). Bar corresponds to 400 nm.

The inner structure of PC vesicular nanosystems was evaluated by SAXS. In the case of ETO and TETO-2 the presence of superposed peaks, with spacing in a ratio of 1:2, revealed the formation of multilamellar vesicles, in agreement with TEM observation, while in the case of TETO-1 and TETO-3, a bilayer form factor scattering pattern was observed, indicating the occurrence of unilamellar vesicles. It is likely that on one hand the presence of P407 could stabilize the multilamellar structure of PC bilayers, while on the other the addition of TW_{80} could affect the multilamellar organization. Conversely, the presence of MG did not affect the structural properties of nanovesicles.

To investigate the suitability of ETO and TETO as delivery systems for MG, the EC values were evaluated by vesicle ultrafiltration and HPLC. As reported in Table 3, EC values were above 71%, following the order TETO-2-MG > TETO-3-MG > ETO-MG >

TETO-1-MG, suggesting that to the highest amount of PC associated to P407 or TW₈₀ could better entrap the lipophilic MG.

Table 3. Entrapment capacity and diffusion coefficients of MG loaded in the indicated forms.

Formulation	EC ^a (%)	F ^b ($\mu\text{g}/\text{cm}^2 \times \text{h} \times 10^3$)	D ^c ($\text{cm}/\text{h} \times 10^3$)
ETO-MG	78	42.03	42.03
TETO-1-MG	71	67.70	67.70
TETO-2-MG	88	36.82	52.32
TETO-3-MG	87	52.32	36.82
Sol-MG	-	73.02	73.02

^a Entrapment capacity; ^b Flux; ^c Diffusion coefficient; Data are the mean of 6 independent Franz cell experiments.

3.3. In Vitro Diffusion Studies

Franz cell experiments were conducted to shed light on the influence of vesicular nanosystem composition on MG diffusion. Figure 2 reports the MG diffusion kinetics from ETO and TETO compared to a solution of MG in ethanol/water (30/70, v/v)

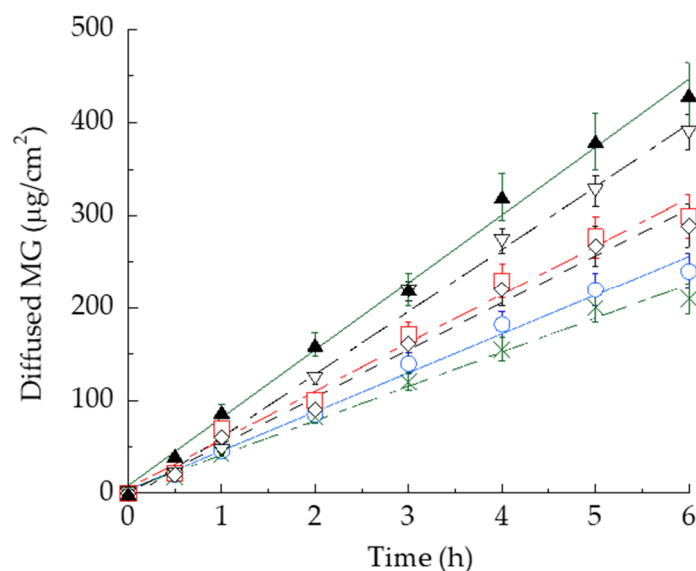


Figure 2. MG diffusion kinetics from ETO-MG (blue circles), TETO-1-MG (open triangles), TETO-2-MG (green crosses), TETO-3-MG (red squares), and Sol-MG (closed triangles), as determined by Franz cell. Experiments were conducted for 6 h. Data are the mean of 6 independent experiments \pm s.d..

In general, vesicular systems controlled MG diffusion with respect to Sol-MG. D values of vesicular systems followed the order TETO-1-MG > TETO-3-MG > ETO-MG > TETO-2-MG (Table 3). Particularly, on one hand the presence of TW₈₀ (TETO-1-MG) increased MG diffusion with respect to plain ETO-MG, while on the other a double amount of PC associated to P407 enabled to halve D of MG (TETO-2-MG). On the basis of the EE of MG and the capability to restrain MG diffusion, TETO-2-MG and TETO-3-MG were selected for biological studies.

3.4. Biological Evaluation

To study the transdermal potential of TETO-2-MG and TETO-3-MG and their protective effect against pollutants, 3D human skin models were employed. Particularly, 4HNE protein adducts levels were evaluated in order to gain information on the protective effect of the encapsulated MG, that is known to counteract the cutaneous O₃-induced oxidative stress damage. 4HNE protein adducts normally occur upon O₃ exposure and represent a marker of lipid peroxidation [14]. Three D human epidermis model is widely accepted to study cutaneous drug permeability, since it accurately mimics the human skin [15]. Namely, after a pretreatment of 3D human skin tissues with TETO-2-MG and TETO-3-MG the tissues were exposed to O₃. The 4HNE protein adducts levels were then evaluated by immunofluorescence staining directly post-exposure and 24 h later. The exposure to O₃ induced a significant increase in 4HNE protein adducts levels with respect to untreated tissues exposed to air. The topical administration of TETO-2-MG and TETO-3-MG induced a halving of 4HNE levels, resulting in protection against oxidative stress promoted by O₃ exposure. The effect has been maintained even 24 h after O₃ exposure, suggesting that the vesicles were able to retain MG and prolong its release. Moreover, since the cutaneous oxidative stress is directly related to inflammation on skin upon pollutants exposure, the release of proinflammatory cytokine IL-1 β was measured in 3D skin models to study the inflammatory conditions under O₃ exposure. The analysis of IL-1 β levels (pg/ml) expressed as AU% in media of 3D skin models treated with TETO-2-MG and TETO-3-MG is reported in Figure 3.

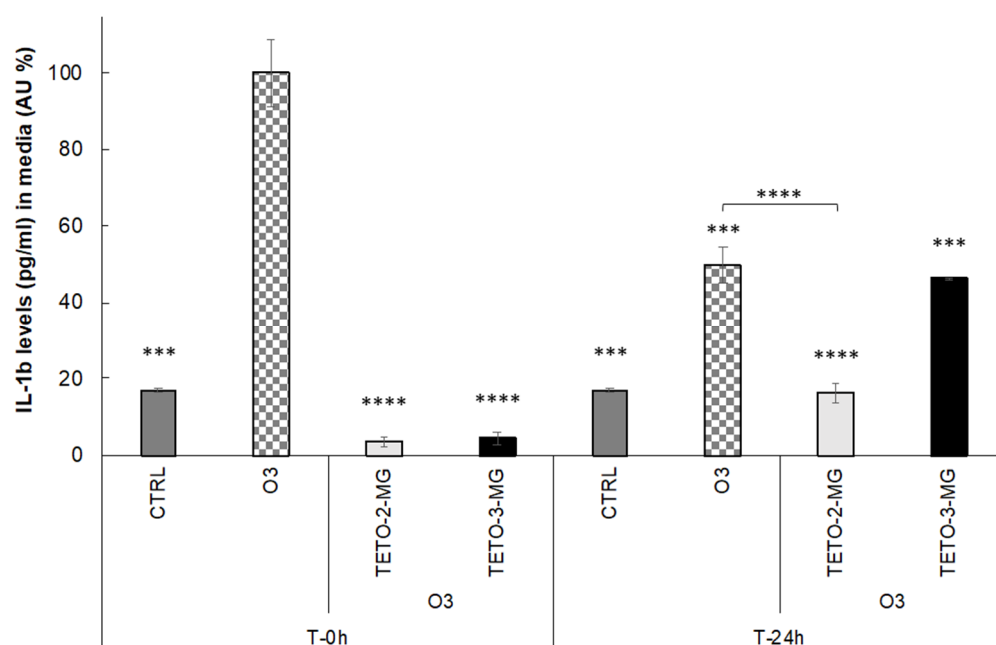


Figure 3. Levels of IL-1 β (pg/mL) in the media of 3D skin models treated with TETO-2-MG and TETO-3-MG analysed using an IL-1 β ELISA kit 0 or 24 h after exposure to O₃ 0.4 ppm for 4 h. Data were normalized with respect to the O₃ sample at 0 h and expressed as arbitrary units (%) \pm SD. Data are the averages of at least three different experiments. *** $p < 0.001$, **** $p < 0.0001$ vs O₃ at T-0 h.

As shown in Figure 3, immediately after exposure to O₃, high levels of IL-1 β were released, confirming the inflammatory status of the skin, as compared to CTRL sample. On the other hand, in the case of TETO-2-MG and TETO-3-MG treatment low levels of IL-1 β were released, suggesting an almost total protection against O₃ damage. Notably, after 24 h, the capability of TETO-2-MG to prevent the O₃ inflammatory damage was even more evident with respect to TETO-3-MG. This effect indicates that TETO-2-MG exerted a

longer MG antiinflammatory effect with respect to TETO-3-MG, in agreement with in vitro diffusion data.

4. Discussion

The preformulatory study evidenced the importance of the choice of components in the design of nanovesicular systems. Indeed, structural features such as mean diameter and morphology of the vesicles, as well as EE of MG, were affected by PC concentration and by the presence of TW₈₀ or P407. In ETO PC self-organized forming the typical multilamellar vesicles, as previously demonstrated [10]. In the presence of TW₈₀, a disordering of the lamellar organization occurs, possibly due to the insertion of the surfactant oleate chain between the lipid bilayer, and to a non-uniform swelling of the aqueous compartments in contact with the polar terminal groups of the polyoxyethylene chains (TETO-1, TETO-3). Conversely, a doubling of PC concentration in the presence of P407 stabilized the multilamellar packing of the vesicles (TETO-2), suggesting that P407 interacts with the surface of PC vesicles differently with respect to TW₈₀, as demonstrated by other authors. Indeed, P407 is a pluronic copolymer, a special kind of non-ionic surfactants, based on a central polyoxypropylene block surrounded by two hydrophilic polyoxyethylene blocks, forming in water spherical polymeric micelles, with a polyoxypropylene hydrophobic core and a hydrophilic PEO screen [16]. It is likely that in the presence of PC the hydrophilic blocks interact with lipid headgroups, whereas the hydrophobic blocks can insert into the central hydrophobic region of the bilayer reducing the lamellar repeat distance. The stabilizing effect of P407 on PC vesicles was previously described by other authors [17,18]. The peculiar structure of TETO-2-MG stabilized by P407 enabled to hamper MG diffusion with respect to the vesicles produced in the presence of TW₈₀ (TETO-1-MG and TETO-3-MG). The ex-vivo results, based on the 3D skin model, well agreed with in vitro findings, demonstrating a prolonged effect of MG in the case of TETO-2-MG and TETO-3-MG. Notably, the skin model is suitable to mimic the skin behavior, being characterized by both the stratum corneum and the epidermic layers, which are the most external layers of the skin, while it avoids the variability related to the use of human skin biopsies. The encouraging results suggest the possibility to further investigate the TETO transdermal potential evaluating by transmission electron microscopy their presence in the different skin layers, such as the deeper epidermis or dermis, employing skin explants.

5. Conclusions

This study has demonstrated the suitability of ETO and TETO as delivery systems for MG. Particularly, the association of surfactants such as P407 to the multilamellar vesicles formed by PC resulted in stable structures suitable to control MG diffusion with respect to vesicles containing TW₈₀. The vesicle size distribution and the EE values of MG were affected by PC concentration and surfactant presence, indicating that the highest amount of PC associated to P407 or TW₈₀ could better entrap the lipophilic MG. Notably, the biological study evidenced that TETO-2-MG and TETO-3-MG can exert a total protection against O₃ damage in 3D skin model. Nonetheless, animal models will be required to evaluate the efficacy of TETO-2-MG and TETO-3-MG in the prevention and treatment of cutaneous conditions related to ox-inflammatory mechanisms.

Author Contributions: Conceptualization, G.V. and E.E.; Data curation, F.F., M.S. and M.G.O.; Formal analysis, F.F., M.B., and A.P.; Funding acquisition, E.E.; Investigation, F.F., M.S. and M.B.; Methodology, E.E. and P.M.; Project administration, G.V. and E.E.; Supervision, G.V. and E.E.; Writing – original draft, E.E. and M.S.; Writing – review & editing, E.E., F.F., G.V., M.S. and R.C.

Funding: This research was funded by the University of Ferrara, FAR 2020.

Data Availability Statement: Not applicable

Acknowledgments: We acknowledge Diamond Light Source for time on Beamline I22 under Proposal SM28022. The authors also acknowledge the kind support provided by Olga Shebanova and Tim Snow.

Conflicts of Interest: The authors declare no conflict of interest. The funders had no role in the design of the study; in the collection, analyses, or interpretation of data; in the writing of the manuscript, or in the decision to publish the results.

References

1. Bălă, G.-P.; Râjnoveanu, R.-M.; Tudorache, E.; Motișan, R.; Oancea, C. Air Pollution Exposure—the (in)Visible Risk Factor for Respiratory Diseases. *Environ. Sci. Pollut. Res.* **2021**, *28*, 19615–19628, doi:10.1007/s11356-021-13208-x.
2. Lim, C.C.; Hayes, R.B.; Ahn, J.; Shao, Y.; Silverman, D.T.; Jones, R.R.; Garcia, C.; Bell, M.L.; Thurston, G.D. Long-Term Exposure to Ozone and Cause-Specific Mortality Risk in the United States. *Am. J. Respir. Crit. Care. Med.* **2019**, *200*, 1022–1031, doi:10.1164/rccm.201806-1161OC.
3. Matkowski, A.; Kus, P.; Goralska, E.; Wozniak, D. Mangiferin – a Bioactive Xanthonoid, Not Only from Mango and Not Just Antioxidant. *MRCM* **2013**, *13*, 439–455, doi:10.2174/1389557511313030011.
4. Telang, M.; Dhulap, S.; Mandhare, A.; Hirwani, R. Therapeutic and Cosmetic Applications of Mangiferin: A Patent Review. *Expert Opin Ther Pat* **2013**, *23*, 1561–1580, doi:10.1517/13543776.2013.836182.
5. Natsheh, H.; Vettorato, E.; Touitou, E. Ethosomes for Dermal Administration of Natural Active Molecules. *CPD* **2019**, *25*, 2338–2348, doi:10.2174/1381612825666190716095826.
6. Ascenso, A.; Raposo, S.; Batista, C.; Cardoso, P.; Mendes, T.; Praça, F.G.; Bentley, M.V.L.B.; Simões, S. Development, Characterization, and Skin Delivery Studies of Related Ultradeformable Vesicles: Transfersomes, Ethosomes, and Transethosomes. *Int. J. Nanomedicine* **2015**, *10*, 5837–5851, doi:10.2147/IJN.S86186.
7. Sguizzato, M.; Ferrara, F.; Hallan, S.S.; Baldisserotto, A.; Drechsler, M.; Malatesta, M.; Costanzo, M.; Cortesi, R.; Puglia, C.; Valacchi, G.; et al. Ethosomes and Transethosomes for Mangiferin Transdermal Delivery. *Antioxidants* **2021**, *10*, 768, doi:10.3390/antiox10050768.
8. Pecora, R. Dynamic Light Scattering Measurement of Nanometer Particles in Liquids. *J. Nanopart. Res.* **2000**, *2*, 123–131, doi:10.1023/A:1010067107182.
9. Barbosa, L.R.S.; Ortore, M.G.; Spinozzi, F.; Mariani, P.; Bernstorff, S.; Itri, R. The Importance of Protein-Protein Interactions on the PH-Induced Conformational Changes of Bovine Serum Albumin: A Small-Angle X-Ray Scattering Study. *Biophys. J.* **2010**, *98*, 147–157, doi:10.1016/j.bpj.2009.09.056.
10. Hallan, S.S.; Sguizzato, M.; Mariani, P.; Cortesi, R.; Huang, N.; Simelière, F.; Marchetti, N.; Drechsler, M.; Ruzgas, T.; Esposito, E. Design and Characterization of Ethosomes for Transdermal Delivery of Caffeic Acid. *Pharmaceutics* **2020**, *12*, 740, doi:10.3390/pharmaceutics12080740.
11. FDA Guidance for Industry: SUPAC-SS: Nonsterile Semisolid Dosage Forms; Scale-Up and Post-Approval Changes: Chemistry, Manufacturing and Controls; In-Vitro Release Testing and In Vivo Bioequivalence Documentation - ECA Academy Available online: <https://www.gmp-compliance.org/guidelines/gmp-guideline/fda-guidance-for-industry-supac-ss-nonsterile-semisolid-dosage-forms-scale-up-and-post-approval-changes-chemistry-manufacturing-> (accessed on 22 July 2021).
12. Ferrara, F.; Pambianchi, E.; Pecorelli, A.; Woodby, B.; Messano, N.; Therrien, J.-P.; Lila, M.A.; Valacchi, G. Redox Regulation of Cutaneous Inflammation by Ozone Exposure. *Free Radic. Biol. Med.* **2020**, *152*, 561–570, doi:10.1016/j.freeradbiomed.2019.11.031.
13. Romani, A.; Cervellati, C.; Muresan, X.M.; Belmonte, G.; Pecorelli, A.; Cervellati, F.; Benedusi, M.; Evelson, P.; Valacchi, G. Keratinocytes Oxidative Damage Mechanisms Related to Airborne Particle Matter Exposure. *Mech. Ageing Dev.* **2018**, *172*, 86–95, doi:10.1016/j.mad.2017.11.007.
14. Pecorelli, A.; Woodby, B.; Prioux, R.; Valacchi, G. Involvement of 4-hydroxy-2-nonenal in Pollution-induced Skin Damage. *Bio-Factors* **2019**, biof.1513, doi:10.1002/biof.1513.
15. Küchler, S.; Strüver, K.; Friess, W. Reconstructed Skin Models as Emerging Tools for Drug Absorption Studies. *Expert Opin. Drug Metab. Toxicol.* **2013**, *9*, 1255–1263, doi:10.1517/17425255.2013.816284.
16. Artzner, F.; Geiger, S.; Olivier, A.; Allais, C.; Finet, S.; Agnely, F. Interactions between Poloxamers in Aqueous Solutions: Micellization and Gelation Studied by Differential Scanning Calorimetry, Small Angle X-Ray Scattering, and Rheology. *Langmuir* **2007**, *23*, 5085–5092, doi:10.1021/la062622p.
17. Chandaroy, P.; Sen, A.; Hui, S.W. Temperature-Controlled Content Release from Liposomes Encapsulating Pluronic F127. *J. Controlled Release* **2001**, *76*, 27–37, doi:10.1016/S0168-3659(01)00429-1.
18. Kostarelos, K.; Luckham, P.F.; Tadros, Th.F. Addition of (Tri-)Block Copolymers to Phospholipid Vesicles: A Study of the Molecular Morphology and Structure by Using Hydrophobic Dye Molecules as Bilayer Probes. *Journal of Colloid and Interface Science* **1997**, *191*, 341–348, doi:10.1006/jcis.1997.4957.